



New Galactic β Lyrae-type Binaries Showing Superorbital Photometric Cycles

Gonzalo Rojas García^{1,2} , Ronald Mennickent² , P. Iwanek³ , P. Gorrini², J. Garcés², I. Soszyński³ , and N. Astudillo-Defru⁴¹Centrum Astronomiczne im. Mikołaja Kopernika (CAMK), PAN, Bartycka 18, 00-716 Warsaw, Poland; gonzrojas@udec.cl²Universidad de Concepción, Departamento de Astronomía, Casilla 160-C, Concepción, Chile³Astronomical Observatory, University of Warsaw, Al. Ujazdowskie 4, PL-00-478 Warszawa, Poland⁴Departamento de Matemática y Física Aplicadas, Universidad Católica de la de Santísima Concepción, Alonso de Rivera 2850, Concepción, Chile

Received 2021 March 15; revised 2021 July 22; accepted 2021 July 24; published 2021 November 16

Abstract

We present the discovery of 32 new double periodic variables (DPVs) located toward the Galactic bulge. We found these objects among the nearly half a million binary stars published by the Optical Gravitational Lensing Experiment project. With this discovery, we increase the number of known DPVs in the Milky Way by a factor of 2. The new set of DPVs contains 31 eclipsing binaries and one ellipsoidal variable star. The orbital periods cover the range from 1.6 to 26 days, while long periods are detected between 47 and 1144 days. Our analysis confirms a known correlation between orbital and long periods that is also observed in similar systems in the Magellanic Clouds.

Unified Astronomy Thesaurus concepts: [Eclipsing binary stars \(444\)](#); [Beta Lyrae stars \(149\)](#); [Double periodic variable stars \(2111\)](#)

1. Introduction

Double periodic variables (DPVs) are a class of semidetached binary systems that have the remarkable characteristic of a secondary long photometric variation in their light curves in addition to the variation due the orbital motion. This class of binaries has been noticed for the first time by Mennickent et al. (2003) after a search for Be-type stars in the Magellanic Clouds. Later, many more similar variables were found in the Magellanic Clouds (Poleski et al. 2010; Pawlak et al. 2013). Previously, some Algols were reported in the literature to have a long periodicity. Kalv (1979) interpreted the 516 day periodicity of RX Cas as pulsations of the Roche-lobe-filling star. Pulsations for the B8 II component of β Lyrae are also suggested by Guinan (1989), although he also mentions possible changes in the structure of the disk. Peters (1994) suggests that the AU Mon long-term light variability is caused by cyclic pulsations of the donor. Studying β Lyrae, Harmanec et al. (1996) considered the 282 day cycle as a possible beat between the 12.9 day orbital period and the 4.7 day period detected in spectroscopy.

Semidetached systems, in particular DPVs, are interacting binaries where mass transfer occurs between the stellar components. The gravitational potential in this configuration can be expressed by the Roche potential (Roche 1873; Kopal 1959), where one of the components (cooler and less massive, the secondary component) overflows its Roche lobe, transferring mass onto the primary component (hotter and more massive, the primary component). As a consequence of the mass transfer, an accretion disk can appear surrounding the primary component. An extensive overview of DPVs has been published by Mennickent (2017). DPVs generally host B-type dwarf primary components of mass between 7 and 10 M_{\odot} and A/F/G-type giant secondary components with masses between 1–3 M_{\odot} . The intrinsic relation between the orbital and long

periods can be expressed by $P_1 \approx 33P_{\text{orb}}$, although single systems can shift from this general tendency appreciably (Mennickent 2017). The origin of the long cycle still is an enigma, although Schleicher & Mennickent (2017) argued that a magnetic dynamo in the donor drives the long cycle. As explained by Mennickent et al. (2016), the physical configuration of these sources is quite similar to those found in classical Algols, but DPVs are hotter and more massive.

From the evolutionary point of view, DPVs can be considered Algols because of their intermediate mass and reversal of the mass ratio, with the less massive component being the more evolved one (Crawford 1955). This in principle puzzling condition was once called “the Algol paradox.” Nowadays, it is unknown why only some Algols display the DPV phenomenon, and is clear that the discovery of new systems will help to better understand the physical processes in close-in binary systems and explain the origin of their superorbital cycles.

Only a few DPVs have been discovered in the Milky Way, compared with significantly larger numbers reported in the Magellanic Clouds (Mennickent et al. 2003; Poleski et al. 2010; Pawlak et al. 2013). It is then expected that several Galactic DPVs remain to be discovered in our galaxy. The context of some photometric surveys still need to be searched for DPVs, e.g., Kepler (Kirk et al. 2016) and the Catalina Survey (Drake et al. 2009). In order to start filling this gap, we searched for new DPVs in the catalog of eclipsing and ellipsoidal binary stars toward the Galactic bulge discovered in the framework of the Optical Gravitational Lensing Experiment (OGLE) project (Soszyński et al. 2016). Here we present the results of this inspection.

2. Observation and Data

We searched for new DPVs in the catalog of more than 450,000 eclipsing and ellipsoidal binary stars published by Soszyński et al. (2016), considering data obtained under phases II, III, and IV of the OGLE project. The data were obtained at the 1.3 m Warsaw Telescope, located at Las Campanas Observatory, Chile, during the years 1997–2015. Images were

Table 1
Newly Discovered Galactic Double Periodic Variables

OGLE ID	I (OGLE) (mag)	V (OGLE) (mag)	$V - I$ (OGLE) (mag)	R.A. (J2000)	Decl. (J2000)
OGLE-BLG-ECL-022295	16.630	18.802	2.172	17:30:11.87	-28:30:05.5
OGLE-BLG-ECL-022845	16.137	19.294	3.157	17:30:30.80	-30:50:26.1
OGLE-BLG-ECL-026467	16.994	19.771	2.777	17:32:08.78	-30:35:27.1
OGLE-BLG-ECL-026993	16.778	19.291	2.513	17:32:20.45	-28:00:25.8
OGLE-BLG-ECL-029922	15.886	18.573	2.687	17:33:18.50	-27:34:55.5
OGLE-BLG-ECL-030962	18.252	21.177	2.925	17:33:35.56	-28:33:39.9
OGLE-BLG-ECL-058684	17.661	20.902	3.241	17:39:53.70	-33:20:44.7
OGLE-BLG-ECL-062890	16.534	18.699	2.165	17:40:45.16	-37:41:37.3
OGLE-BLG-ECL-072154	15.940	17.387	1.447	17:42:27.03	-21:37:33.7
OGLE-BLG-ECL-076504	16.789	18.727	1.938	17:43:10.65	-34:29:42.5
OGLE-BLG-ECL-083987	18.042	21.274	3.232	17:44:18.78	-32:52:45.2
OGLE-BLG-ECL-101353	17.118	19.719	2.601	17:46:41.42	-21:52:56.1
OGLE-BLG-ECL-116536	16.543	17.521	0.978	17:48:46.77	-35:03:15.6
OGLE-BLG-ECL-132549	17.108	20.168	3.060	17:50:48.55	-30:40:20.0
OGLE-BLG-ECL-137478	16.382	18.899	2.517	17:51:20.86	-22:51:19.5
OGLE-BLG-ECL-143267	16.613	19.050	2.437	17:51:53.66	-32:52:22.0
OGLE-BLG-ECL-184474	17.495	21.290	3.795	17:55:23.67	-22:09:16.3
OGLE-BLG-ECL-186594	16.253	17.663	1.410	17:55:34.15	-32:49:34.2
OGLE-BLG-ECL-189682	16.292	18.676	2.384	17:55:50.33	-31:31:09.1
OGLE-BLG-ECL-196052	16.097	18.809	2.712	17:56:21.93	-20:31:35.7
OGLE-BLG-ECL-198013	17.435	20.263	2.828	17:56:32.45	-21:34:05.7
OGLE-BLG-ECL-201730	15.586	16.467	0.881	17:56:51.04	-35:09:18.6
OGLE-BLG-ECL-210744	16.803	17:56:51.11	-31:32:41.7
OGLE-BLG-ECL-222537	15.737	17:58:38.36	-34:25:27.4
OGLE-BLG-ECL-271003	17.592	18.375	0.783	18:03:00.42	-28:39:53.7
OGLE-BLG-ECL-275974	15.866	17.637	1.771	18:03:27.99	-27:43:43.1
OGLE-BLG-ECL-279247	16.527	19.327	2.800	18:03:45.59	-26:57:40.5
OGLE-BLG-ECL-327914	15.308	17.584	2.276	18:08:32.17	-25:29:53.2
OGLE-BLG-ECL-328103	15.598	17.168	1.570	18:08:33.24	-29:58:07.4
OGLE-BLG-ECL-331967	15.786	17.309	1.523	18:08:59.52	-26:36:48.5
OGLE-BLG-ECL-369067	15.786	17.749	1.963	18:13:28.58	-23:35:56.8
OGLE-BLG-ELL-024487	14.353	15.186	0.833	18:18:18.63	-28:07:26.6

taken in two filters, V and I . The data reduction and calibrations are described in Udalski et al. (2015). Since 2010 until today the OGLE-IV project regularly has observed about 400 million stars in 182 deg^2 of the densest regions of the Galactic bulge. The search for eclipsing variables was based primarily on the OGLE-IV data. The catalog includes objects with magnitudes $12 < I < 21 \text{ mag}$ and $13 < V < 21.7 \text{ mag}$. The CCD saturates at about 13 mag in the I band, while the faintest stars in the OGLE database have $I \approx 21 \text{ mag}$. The typical photometric uncertainty for an individual measurement of a bright star ($I < 14 \text{ mag}$) is about 0.005 mag.

3. Methodology

3.1. Long-period Search and Light-curve Disentangling

In order to find the secondary photometric variation, and consequently a new DPV candidate, we used several analysis tools. We subtracted the orbital periodic contribution provided by the catalog using Fourier analysis and worked with the code written by the late Zbigniew Kołaczkowski and explained by Mennickent et al. (2012). This method uses the frequency associated with the orbital period, and a fixed number of harmonics in order to recreate the contribution of luminosity variation due to the orbital motion of the system. After this procedure, the fitted Fourier approximated light curve is subtracted from the data in order to have only the residuals.

Those residuals were analyzed using the generalized Lomb–Scargle (GLS) periodogram (Zechmeister & Kürster 2009). This algorithm uses the principles of the Lomb (1976) and Scargle (1982) periodograms with some modifications, such as the addition of a displacement in the adjustment of the fit function and the consideration of measurement errors. Compared with the classical periodogram, it gives us more precise frequencies and a better determination of the amplitudes. The phase dispersion minimization algorithm (Stellingwerf 1978) allowed us to confirm the second periodicity. Considering the distribution of DPVs around the straight line $P_l = 33 P_o$ (Mennickent 2017), we considered as DPV candidates those systems whose long periods are between the branches $P_{l\max} = 38.74 P_o + 32.95 \text{ days}$ and $P_{l\min} = 38.74 P_o - 192.05 \text{ days}$, where most of the DPVs are expected to be found. To determine those constraints, we perform a linear regression to the previous 26 Galactic DPVs not passing through the origin of the parametric system (as the $P_l = 33 P_o$ relation suggests). Later we moved the mentioned interpolation along the perpendicular direction of its position. Thus, at this first stage we excluded (likely very few) systems with extreme P_l/P_o ratios. The V , I colors are obtained from the OGLE online catalogs, except in Table 4 where they are from the analyzed time series. The periods reported here were calculated considering all photometric data available until 2019 October.

Table 2
Orbital Period, Long Period, and Period Ratio of Each DPV with Their Respective Errors

Name	P_{orb} (days)	P_{long} (days)	$P_{\text{long}}/P_{\text{orb}}$
OGLE-BLG-ECL-022295	14.678034 ± 0.000416	466.51 ± 1.40	31.78 ± 0.10
OGLE-BLG-ECL-022845	19.715796 ± 0.001462	601.64 ± 2.51	30.52 ± 0.13
OGLE-BLG-ECL-026467	20.78303 ± 0.000688	658.81 ± 4.33	31.70 ± 0.21
OGLE-BLG-ECL-026993	14.761416 ± 0.000590	413.70 ± 1.25	28.03 ± 0.08
OGLE-BLG-ECL-029922	8.107938 ± 0.000074	312.70 ± 0.75	38.57 ± 0.09
OGLE-BLG-ECL-030962	14.883752 ± 0.000818	485.73 ± 2.81	32.63 ± 0.19
OGLE-BLG-ECL-058684	21.70324 ± 0.001888	793.38 ± 4.11	36.56 ± 0.19
OGLE-BLG-ECL-062890	16.66844 ± 0.006358	574.87 ± 18.58	34.49 ± 1.11
OGLE-BLG-ECL-072154	15.04791 ± 0.000850	459.39 ± 1.51	30.53 ± 0.10
OGLE-BLG-ECL-076504	1.598269 ± 0.000026	50.32 ± 0.02	31.48 ± 0.01
OGLE-BLG-ECL-083987	11.017538 ± 0.000586	245.50 ± 1.02	22.28 ± 0.09
OGLE-BLG-ECL-101353	12.997544 ± 0.001022	438.17 ± 8.51	33.71 ± 0.65
OGLE-BLG-ECL-116536	7.712738 ± 0.000144	256.20 ± 0.29	33.22 ± 0.04
OGLE-BLG-ECL-132549	12.17615 ± 0.000216	353.20 ± 0.45	29.01 ± 0.04
OGLE-BLG-ECL-137478	21.46779 ± 0.003338	773.80 ± 6.85	36.04 ± 0.312
OGLE-BLG-ECL-143267	16.803896 ± 0.000312	519.95 ± 0.68	30.94 ± 0.04
OGLE-BLG-ECL-184474	18.64614 ± 0.002076	571.60 ± 4.82	30.66 ± 0.26
OGLE-BLG-ECL-186594	1.592281 ± 0.000025	46.98 ± 0.04	29.50 ± 0.03
OGLE-BLG-ECL-189682	17.222906 ± 0.000260	566.25 ± 0.72	32.88 ± 0.04
OGLE-BLG-ECL-196052	25.744828 ± 0.004494	1091.06 ± 20.56	42.38 ± 0.80
OGLE-BLG-ECL-198013	14.80092 ± 0.001594	521.81 ± 4.87	35.26 ± 0.33
OGLE-BLG-ECL-201730	9.401168 ± 0.00043	291.63 ± 0.55	31.02 ± 0.06
OGLE-BLG-ECL-210744	12.600516 ± 0.000106	299.57 ± 0.22	23.77 ± 0.02
OGLE-BLG-ECL-222537	15.273438 ± 0.000528	419.40 ± 0.62	27.46 ± 0.04
OGLE-BLG-ECL-271003	1.718797 ± 0.000018	37.84 ± 0.02	22.02 ± 0.01
OGLE-BLG-ECL-275974	15.053288 ± 0.00022	451.22 ± 0.37	29.97 ± 0.02
OGLE-BLG-ECL-279247	18.180322 ± 0.00014	526.07 ± 1.35	28.94 ± 0.07
OGLE-BLG-ECL-327914	19.42795 ± 0.000588	681.60 ± 1.42	35.08 ± 0.07
OGLE-BLG-ECL-328103	14.046314 ± 0.000382	414.58 ± 0.52	29.52 ± 0.04
OGLE-BLG-ECL-331967	10.293578 ± 0.00008	374.77 ± 0.29	36.41 ± 0.03
OGLE-BLG-ECL-369067	24.735716 ± 0.007972	827.92 ± 15.42	33.47 ± 0.62
OGLE-BLG-ELL-024487	19.1256 ± 0.001004	605.06 ± 4.31	31.64 ± 0.23

4. Results

4.1. New DPVs

In Table 1, we provide the list of 32 new DPVs including coordinates, magnitudes, and $V-I$ colors. In Table 2 we provide the orbital and long periods and period ratio. This ratio has an average of 31.9 and a standard deviation of 4.4, calculated using the new and previously found galactic DPVs (58 in total). The new DPVs span an orbital period range of 1.6–26 days and a range of long-cycle lengths of 47–1144 days. We increased the number of known DPVs in the Milky Way by a factor of 2.

4.2. Gaia Identifications, Reddening, and Extinction

The location of the newly discovered DPVs in the direction of the Galactic bulge (see Figure 1) causes the light from the objects to be strongly reddened by unevenly distributed interstellar matter (Nataf et al. 2013; Iwanek et al. 2019).

We cross-matched our list of new DPVs with Gaia DR2 within a radius of 0.4 arcsec. We found 31 out of 32 objects, missing only OGLE-BLG-ECL-030962. To obtain reddening and extinction we made several assumptions: (1) If the parallax is negative in Gaia DR2 we assumed that the object is far away, and we put “NA” in the parallax and error for this object, and we assumed that this object is in the bulge, at a distance of 8.0 kpc. (2) If parallax p_i is measured not so accurately ($\sigma_{p_i}/p_i > 0.2$), we also put “NA” in the parallax and error for

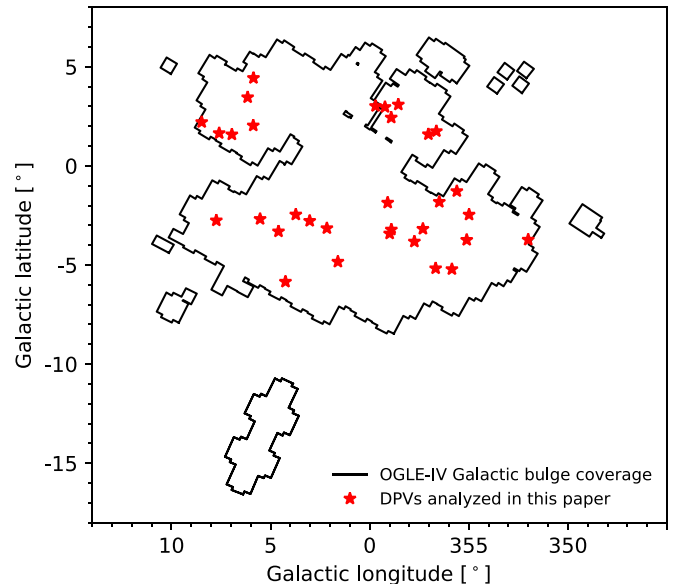


Figure 1. Distribution of 32 newly discovered DPVs systems (marked with red asterisks) in the sky. The black solid line presents the OGLE-IV Galactic bulge coverage.

this object, and again we have assumed a distance to this object of 8.0 kpc. (3) For the object that is missing in Gaia DR2, viz. OGLE-BLG-ECL-030962, we put also “NA” in the parallax and error columns, and a distance of 8.0 kpc. (4) Only three

Table 3
Supplementary Data for New Double Periodic Variables

Object	Gal. Long. (deg)	Gal. Lat. (deg)	p^a (mas)	p Error (mas)	d^b (kpc)	A_V^c (mag)	A_I^c (mag)	$E(V - I)^c$ mag	A_V^d (mag)	A_I^d (mag)	$E(V - I)^d$ (mag)
OGLE-BLG-ECL-022295	358.557628	3.089058	-0.2414	0.4955	8.000	NA	NA	NA	3.591	1.971	1.620
OGLE-BLG-ECL-022845	356.638929	1.746973	0.1505	0.13462	8.000	NA	NA	NA	5.373	2.949	2.424
OGLE-BLG-ECL-026467	357.040308	1.590201	0.069	0.4050	8.000	NA	NA	NA	4.358	2.392	1.966
OGLE-BLG-ECL-026993	359.230521	2.964263	0.1195	0.3709	8.000	NA	NA	NA	4.042	2.219	1.824
OGLE-BLG-ECL-029922	359.704265	3.015798	0.4717	0.1379	8.000	NA	NA	NA	4.599	2.525	2.075
OGLE-BLG-ECL-030962	358.915140	2.431787	NA	NA	8.000	NA	NA	NA	4.582	2.515	2.067
OGLE-BLG-ECL-058684	355.605523	-1.278726	0.2229	0.3750	8.000	NA	NA	NA	5.115	2.807	2.307
OGLE-BLG-ECL-062890	352.005548	-3.728611	NA	NA	8.000	NA	NA	NA	3.198	1.756	1.443
OGLE-BLG-ECL-072154	5.864432	4.430295	1.668	0.2928	0.599	2.359	1.296	1.063	0.800	0.439	0.361
OGLE-BLG-ECL-076504	354.988326	-2.463740	-0.0921	0.1939	8.000	3.179	1.743	1.436	2.990	1.641	1.349
OGLE-BLG-ECL-083987	356.489859	-1.819114	NA	NA	8.000	NA	NA	NA	5.794	3.180	2.614
OGLE-BLG-ECL-101353	6.157766	3.456031	0.0847	0.2451	8.000	NA	NA	NA	3.343	1.835	1.508
OGLE-BLG-ECL-116536	355.106546	-3.737345	0.6732	0.2998	8.000	1.932	1.076	0.856	1.981	1.087	0.894
OGLE-BLG-ECL-132549	359.094035	-1.860209	NA	NA	8.000	4.527	2.472	2.055	4.176	2.292	1.884
OGLE-BLG-ECL-137478	5.875026	2.032450	-0.0043	0.1786	8.000	3.794	2.089	1.705	3.361	1.845	1.516
OGLE-BLG-ECL-143267	357.316377	-3.179985	0.3756	0.2267	8.000	3.202	1.780	1.422	2.954	1.621	1.332
OGLE-BLG-ECL-184474	6.953516	1.582069	-0.1959	0.3676	8.000	NA	NA	NA	4.530	2.486	2.043
OGLE-BLG-ECL-186594	357.746645	-3.822959	0.0306	0.1319	8.000	2.371	1.302	1.069	2.326	1.277	1.049
OGLE-BLG-ECL-189682	358.908536	-3.217529	0.1511	0.1980	8.000	3.071	1.659	1.412	2.583	1.418	1.165
OGLE-BLG-ECL-196052	8.475284	2.205042	-0.0218	0.1831	8.000	NA	NA	NA	3.520	1.932	1.588
OGLE-BLG-ECL-198013	7.594280	1.646958	0.5006	0.4056	8.000	NA	NA	NA	5.215	2.862	2.353
OGLE-BLG-ECL-201730	355.853858	-5.213840	-0.01184	0.2476	8.000	1.32	0.736	0.584	1.566	0.859	0.706
OGLE-BLG-ECL-210744	358.994402	-3.417298	NA	NA	8.000	3.019	1.662	1.357	2.715	1.490	1.225
OGLE-BLG-ECL-222537	356.674097	-5.171711	0.1177	0.1708	8.000	1.204	0.651	0.553	1.318	0.723	0.595
OGLE-BLG-ECL-271003	2.160899	-3.148999	0.1610	0.5863	8.000	1.836	0.992	0.844	1.530	0.840	0.690
OGLE-BLG-ECL-275974	3.027708	-2.778162	0.2200	0.1463	8.000	2.082	1.109	0.973	1.972	1.083	0.890
OGLE-BLG-ECL-279247	3.729224	-2.458737	-0.6954	0.2330	8.000	3.165	1.698	1.467	2.494	1.369	1.125
OGLE-BLG-ECL-327914	5.530497	-2.682171	NA	NA	8.000	2.747	1.499	1.248	2.760	1.515	1.245
OGLE-BLG-ECL-328103	1.605719	-4.838699	NA	NA	8.000	1.396	0.768	0.628	1.495	0.820	0.674
OGLE-BLG-ECL-331967	4.601795	-3.310174	0.2199	0.1019	8.000	2.366	1.263	1.103	2.087	1.146	0.942
OGLE-BLG-ECL-369067	7.738126	-2.755571	-0.0521	0.1387	8.000	NA	NA	NA	3.335	1.830	1.504
OGLE-BLG-ELL-024487	4.249912	-5.847587	0.1452	0.0564	8.000	NA	NA	NA	1.106	0.607	0.499

Notes. See the text for details.

^a Parallaxes from GDR2.

^b Distances calculated using the GDR2 parallax.

^c Extinction and reddening from Nataf et al. (2013).

^d Extinction and reddening from mw dust.

objects have nonnegative and accurate parallax measurements, so for them we have calculated distances resulting from the parallax. As a result, we identified 31 DPVs as members of the Galactic bulge, and 1 DPV that is located closer to the Sun, and does not belong to the Galactic bulge, but it is projected on the field of view of the bulge, viz. OGLE-BLG-ECL-072154, located at 0.599 kpc.

In the first step we obtained reddening and extinction using Nataf’s maps. These maps are made using red clump stars from the bulge, using OGLE-III data. Using these maps we automatically make the assumption that the object for which we measure extinction and reddening is located in the bulge, behind all the dust. These maps are good enough for distant stars (which are located more or less in the bulge). The “NA” label in columns 7–9 (Nataf’s reddening and extinction) means that toward these directions there are no measurements available.

We calculated dereddened colors and magnitudes defined as

$$I_0 = I - A_I, \quad (1)$$

$$(V - I)_0 = (V - I) - E(V - I), \quad (2)$$

where A_I and $E(V - I)$ are the I -band extinction and the color excess, respectively. Table 3 provides a compilation of our results about Gaia identification, extinction, and reddening. Additional information about the analyzed light curves is given in Table 4.

5. Discussion

In Figure 2 we show the correlation between orbital and long periods for previously known Galactic DPVs supplemented with new discoveries described in this paper. It is clear that the new systems follow the same general tendency, in the sense of a monotonic increase of the orbital period with a long-cycle length. Most of the new systems have periods longer than 10 days. MNIC V99 reported by Nikolay Mishevskiy in VSX, has a period ratio of 21.67, similar to β Lyrae (21.25). It is a member of the open cluster NGC 146, and was classified as a classical Be star of spectral type B3V by Mathew & Subramaniam (2011). The period distributions are shown in Figure 3. The distribution of dereddened $(V - I)_0$ colors and magnitudes are given in Figure 4. Most of the systems have

Table 4
Observational Data for Each DPV^a

DPV OGLE-BGL-	Filter	N_{data}	T_i	T_f	\bar{m} ag	σ mag
<i>ECL-022295</i>	<i>I</i>	1172	5265.81414	8763.57341	16.695	0.067
$V - I = 2.172 \pm 0.019$	<i>V</i>	65	5267.80384	8726.61207	18.867	0.080
<i>ECL-022845</i>	<i>I</i>	922	5309.86179	8783.52539	16.277	0.212
$V - I = 3.187 \pm 0.029$	<i>V</i>	45	5641.85396	8728.57093	19.464	0.419
<i>ECL-026467</i>	<i>I</i>	942	5307.81611	8783.52539	17.059	0.060
$V - I = 2.789 \pm 0.037$	<i>V</i>	45	5641.85396	8728.57093	19.848	0.065
<i>ECL-026993</i>	<i>I</i>	1034	5376.66303	8763.57341	16.920	0.190
$V - I = 2.574 \pm 0.033$	<i>V</i>	60	5267.80384	8726.61207	19.493	0.332
<i>ECL-029922</i>	<i>I</i>	7212	5265.81251	8783.51337	15.920	0.035
$V - I = 2.689 \pm 0.014$	<i>V</i>	211	5267.80162	8763.54658	18.609	0.037
<i>ECL-030962</i>	<i>I</i>	1149	5288.86318	8783.52846	18.401	0.247
$V - I = 3.237 \pm 0.176$	<i>V</i>	44	5288.84266	8741.59303	21.638	0.376
<i>ECL-058684</i>	<i>I</i>	744	5306.76435	8762.52513	17.800	0.220
$V - I = 3.426 \pm 0.157$	<i>V</i>	28	5740.70369	8695.76659	21.227	0.274
<i>ECL-062890</i>	<i>I</i>	172	5385.58089	6737.82676	16.687	0.174
$V - I = 2.239 \pm 0.027$	<i>V</i>	6	5694.72823	6534.56085	18.926	0.105
<i>ECL-072154</i>	<i>I</i>	549	2124.50928	7817.83566	16.048	0.202
$V - I = 1.451 \pm 0.010$	<i>V</i>	29	4757.5214	7269.53372	17.500	0.079
<i>ECL-076504</i>	<i>I</i>	1820	2116.77407	8750.60203	16.810	0.136
$V - I = 1.952 \pm 0.023$	<i>V</i>	59	3480.8138	8716.54655	18.762	0.068
<i>ECL-083987</i>	<i>I</i>	926	5378.57053	8762.51912	18.217	0.257
$V - I = 3.252 \pm 0.142$	<i>V</i>	53	5642.81836	8716.54874	21.469	0.308
<i>ECL-101353</i>	<i>I</i>	659	5265.84296	7683.50095	17.261	0.187
$V - I = 2.696 \pm 0.050$	<i>V</i>	31	5275.88529	7284.50657	19.957	0.378
<i>ECL-116536</i>	<i>I</i>	1959	2115.78469	8763.57847	16.594	0.167
$V - I = 1.043 \pm 0.018$	<i>V</i>	79	3478.8164	8718.49908	17.637	0.399
<i>ECL-132549</i>	<i>I</i>	8040	2125.56122	8787.51017	17.172	0.131
$V - I = 3.140 \pm 0.079$	<i>V</i>	169	3476.85723	8728.5651	20.312	0.219
<i>ECL-137478</i>	<i>I</i>	536	5265.85454	7660.52945	16.503	0.188
$V - I = 2.532 \pm 0.035$	<i>V</i>	24	5276.85882	7226.66062	19.035	0.102
<i>ECL-143267</i>	<i>I</i>	3161	551.8965	8783.55044	16.753	0.196
$V - I = 2.469 \pm 0.027$	<i>V</i>	174	1021.77345	8725.4965	19.222	0.306
<i>ECL-184474</i>	<i>I</i>	397	5265.86046	7667.49853	17.648	0.180
$V - I = 3.920 \pm 0.186$	<i>V</i>	11	5276.86706	7198.70108	21.568	0.342
<i>ECL-186594</i>	<i>I</i>	1934	5260.86866	8755.59956	16.337	0.100
$V - I = 1.421 \pm 0.012$	<i>V</i>	156	5266.85076	8722.52336	17.758	0.124
<i>ECL-189682</i>	<i>I</i>	4097	2125.53977	8783.5535	16.413	0.143
$V - I = 2.419 \pm 0.021$	<i>V</i>	161	3476.83803	8724.57564	18.832	0.245
<i>ECL-19605</i>	<i>I</i>	389	5265.85896	7666.5734	16.227	0.152
$V - I = 2.669 \pm 0.019$	<i>V</i>	13	5276.86496	7197.73354	18.896	0.100
<i>ECL-198013</i>	<i>I</i>	385	5265.85896	7666.5734	17.585	0.186
$V - I = 2.915 \pm 0.069$	<i>V</i>	13	5276.86496	7197.73354	20.500	0.410
<i>ECL-201730</i>	<i>I</i>	768	2115.7781	7673.55067	15.719	0.255
$V - I = 0.891 \pm 0.009$	<i>V</i>	40	4686.58622	7252.5753	16.610	0.309
<i>ECL-210744</i>	<i>I</i>	19179	2072.6039	8787.51326	16.969	0.283
<i>ECL-222537</i>	<i>I</i>	524	2116.78882	8617.9366	15.880	0.197
$V - I = 1.219 \pm 0.010$	<i>V</i>	3	3480.83224	4916.88887	17.099	0.054
<i>ECL-271003</i>	<i>I</i>	15831	551.84063	8787.51786	17.602	0.139
$V - I = 0.817 \pm 0.025$	<i>V</i>	247	1300.6775	8742.58799	18.419	0.154

Table 4
(Continued)

DPV OGLE-BGL-	Filter	N_{data}	T_i	T_f	\bar{m} ag	σ mag
<i>ECL-275974</i>	<i>I</i>	8864	2127.48967	8787.51634	16.013	0.214
$V - I = 1.801 \pm 0.011$	<i>V</i>	217	3476.79531	8742.58592	17.813	0.341
<i>ECL-279247</i>	<i>I</i>	8885	2127.51889	8787.51634	16.619	0.080
$V - I = 2.814 \pm 0.029$	<i>V</i>	217	3476.81034	8742.58592	19.433	0.088
<i>ECL-327914</i>	<i>I</i>	2341	2127.60225	8763.5681	15.395	0.104
$V - I = 2.307 \pm 0.009$	<i>V</i>	187	4705.53655	8723.52314	17.702	0.191
<i>ECL-328103</i>	<i>I</i>	1135	2125.61109	8782.55958	15.724	0.181
$V - I = 1.602 \pm 0.010$	<i>V</i>	55	4703.51861	8724.5801	17.326	0.307
<i>ECL-331967</i>	<i>I</i>	3480	551.80801	8763.5696	15.922	0.169
$V - I = 1.575 \pm 0.011$	<i>V</i>	170	607.91592	8725.56589	17.496	0.267
<i>ECL-369067</i>	<i>I</i>	289	5278.90253	7684.52047	15.904	0.282
$V - I = 1.927 \pm 0.014$	<i>V</i>	9	5662.82138	7221.64591	17.831	0.053
<i>ELL-024487</i>	<i>I</i>	475	2463.60617	7672.54903	14.402	0.042

Note.

^a Initial and final dates of time series are given (HJD 2,450,000). *V*, *I* is the uncorrected color obtained from the average magnitudes.

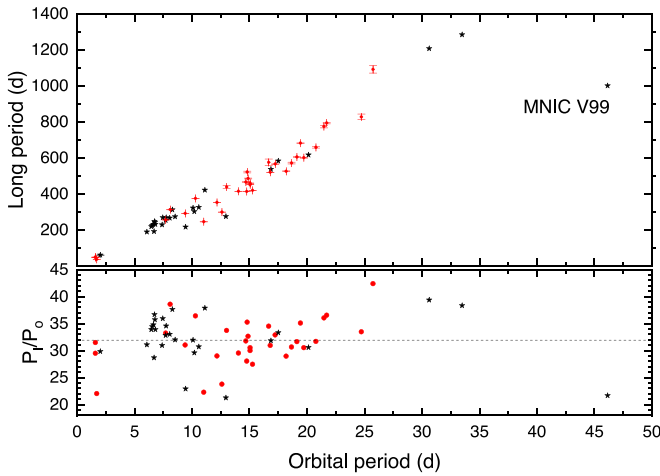


Figure 2. Long period and period ratio vs. orbital period for Galactic DPVs. The new DPVs reported in this paper are shown by dots while the rest, marked with asterisks, are listed in Mennickent (2017), Rosales & Mennickent (2018, 2019), and the VSX database (<https://www.aavso.org/vsx/>). MNIC V99, reported by Nikolay Mishevskiy in VSX, has a period ratio of 21.67, similar to β Lyrae (21.25). The average $P_1/P_0 = 31.9$ is indicated.

brightness I_0 between 12 and 15 mag, while the $(V - I)_0$ colors span a range between 0.0 and 1.8.

Some examples of light curves are given in Figure 5.⁵ They show typical orbital eclipsing light curves of β Lyrae type, i.e., with rounded light curve segments between eclipses, as a result of the proximity among the stars and the gravitational deformation of the less massive component. In Figure 6 we show the color–magnitude diagram constructed with dereddened colors and magnitudes along with PARSEC-COLIBRI stellar isochrones for solar metallicity including the TP-AGB phase (Marigo et al. 2017). Considering that the stars in the Galactic bulge of the Milky Way have a broad range of metallicity, $-3.0 < [\text{Fe}/\text{H}] < 1$ dex (Ness & Freeman 2016),

⁵ The full data sample of discovered DPVs is available at <http://www.astro.uw.edu.pl/ogle/ogle4/OCVS/blg/dpv/>.

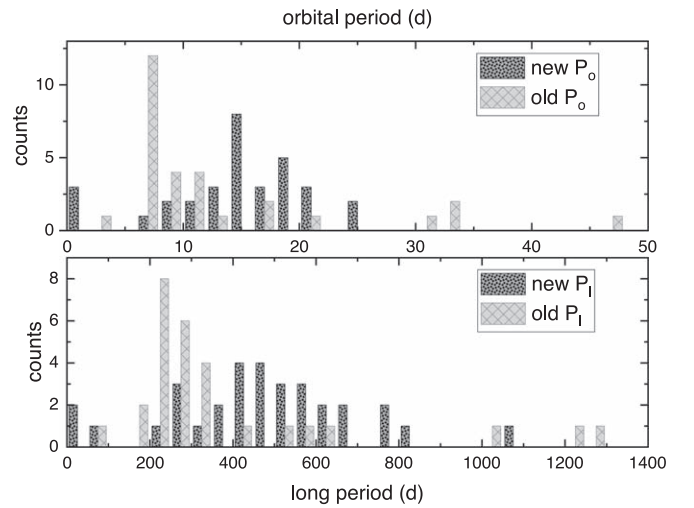


Figure 3. Period distribution for Galactic DPVs.

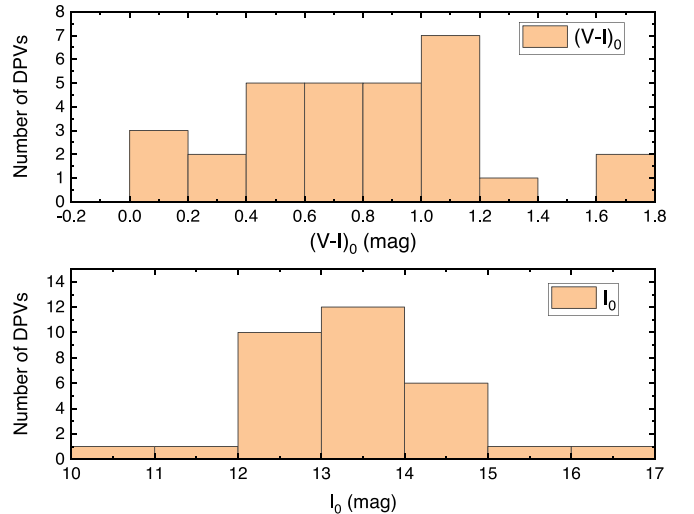


Figure 4. Dereddened color and magnitude distributions for Galactic DPVs.

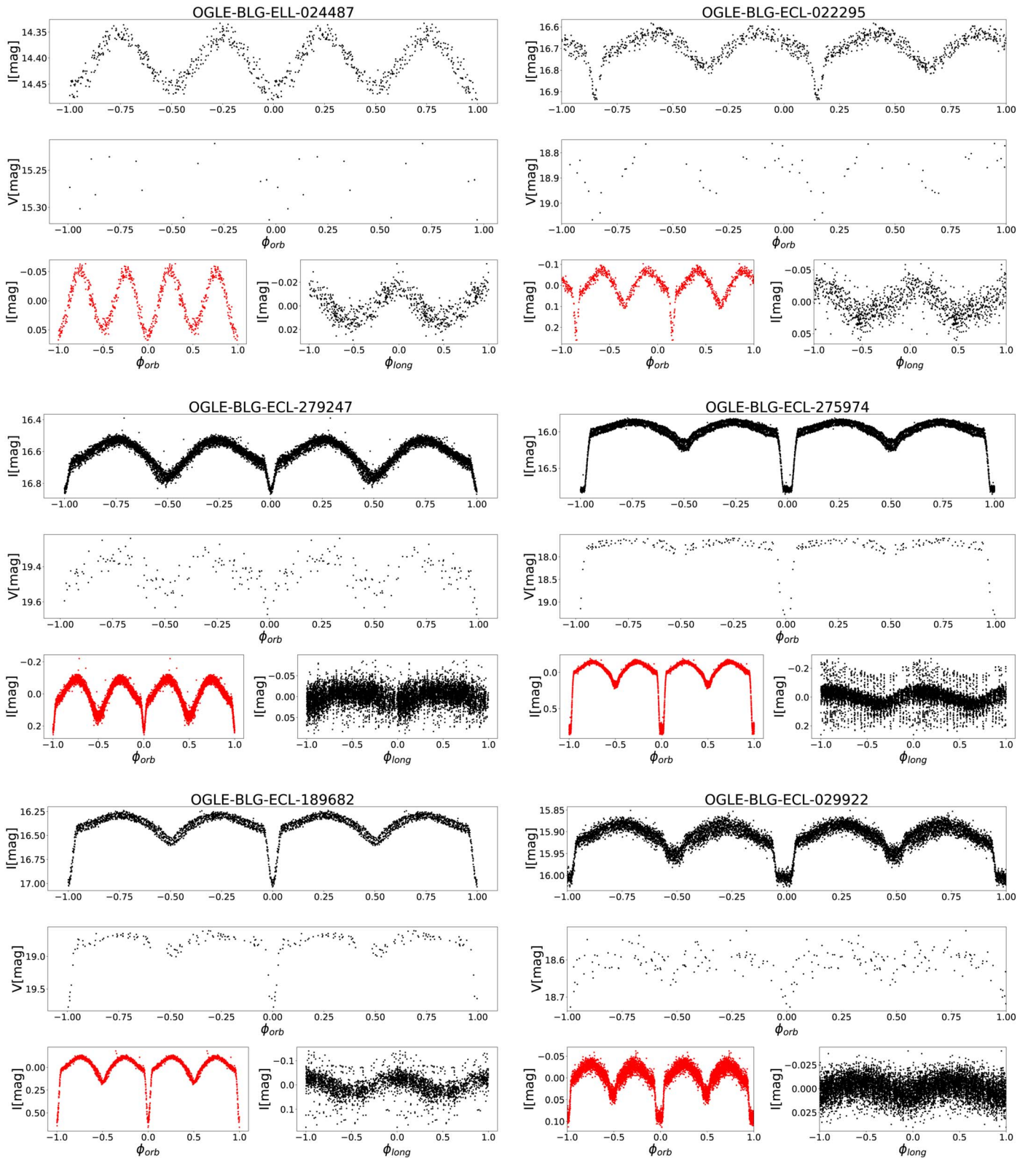


Figure 5. Examples of light curves. Upper: observed light curve. Bottom left: disentangled orbital light curves. Bottom right: disentangled long-cycle light curve. Visit <http://www.astrouw.edu.pl/ogle/ogle4/OCVS/blg/dpv/> for the complete data sample.

we compared our DPVs with isochrones of a representative population of solar metallicity single stars, expecting to infer only general highlights for our DPV population. Keeping in mind that mass transfer usually modifies the evolution of the close binary components, it is apparent that the newly

discovered DPV population is located far from the main-sequence placement. This can be explained if the DPV $V-I$ colors are dominated by the cool mass-transferring giant star. The most extreme red colors in OGLE-BLG-ECL-184474 and OGLE-BLG-ECL-279247 might be explained by light

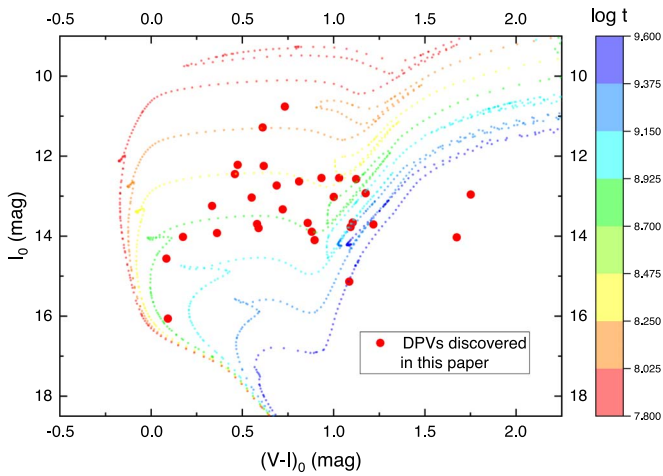


Figure 6. Dereddened color–magnitude diagram for the new DPVs marked with red dots. We plot PARSEC-COLIBRI stellar isochrones for solar metallicity including the TP-AGB phase (Marigo et al. 2017). Isochrones are marked with dotted lines for different values of $\log t$ (Gyr).

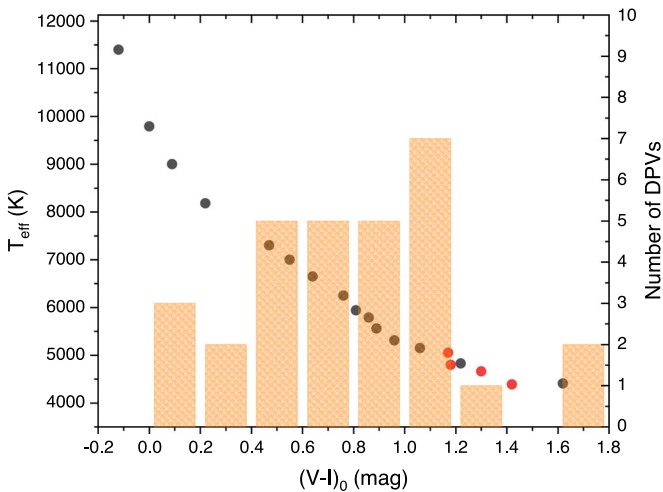


Figure 7. Histogram of colors of new DPVs compared with colors of dwarfs (black dots) and giants (red dots) of different effective temperatures from Cox (2000).

emission from cool circumstellar material, a large accretion disk for instance.

We compare DPV colors with those presented in single giant and dwarf stars (Figure 7). If the donor dominates the system light, then their temperatures are in the range of 11,000–4000 K, corresponding to spectral types \sim B8–K8. It is likely that the true range is in fact narrower, since infrared excess due to circumstellar matter could explain part of the redder colors, while the bluer ones might be influenced by hot and luminous primary components.

6. Summary

We have found 32 new binaries of the DPV type, doubling the number of known DPVs in the Milky Way. Most of the new DPVs are located in the Galactic bulge. We determined

orbital periods and long-cycle periods for all of them and provide coordinates, color excess, and I , $V - I$ information. The I_0 versus $(V - I)_0$ distribution suggests a binary population where the light is dominated by cool giant secondaries and circumstellar matter. Some of the new systems show total eclipses, and are candidates for precise modeling in future investigations.

G.R.G. acknowledges the financial support of the National Science Centre, Poland (NCN) under the project No. 2017/26/A/ST9/00446. R.E.M. acknowledges support by the BASAL Centro de Astrofísica y Tecnologías Afines (CATA) PFB-06/2007 and FONDECYT 1190621. P.I. acknowledges the financial support of the Polish National Science Centre through the PRELUDIUM grant No. 2019/35/N/ST9/02474. The OGLE project has received funding from Polish National Science Centre grant MAESTRO No. 2014/14/A/ST9/00121. N. A.-D. acknowledges the support of FONDECYT project 3180063. J.G. acknowledges ANID project 21202285.

ORCID iDs

Gonzalo Rojas García  <https://orcid.org/0000-0001-9266-3036>

Ronald Mennickent  <https://orcid.org/0000-0002-6245-0264>

P. Iwanek  <https://orcid.org/0000-0002-6212-7221>

I. Soszyński  <https://orcid.org/0000-0002-7777-0842>

References

- Cox, A. N. 2000, in *Allen’s Astrophysical Quantities*, ed. A. N. Cox (4th ed.; New York: AIP)
- Crawford, J. A. 1955, *ApJ*, **121**, 71
- Drake, A. J., Djorgovski, S. G., Mahabal, A., et al. 2009, *ApJ*, **696**, 870
- Guinan, E. F. 1989, *SSRv*, **50**, 35
- Harmanec, P., Morand, F., Bonneau, D., et al. 1996, *A&A*, **312**, 879
- Iwanek, P., Soszyński, I., Skowron, J., et al. 2019, *ApJ*, **879**, 114
- Kalv, P. 1979, *TarOT*, **58**, 3
- Kirk, B., Conroy, K., Prša, A., et al. 2016, *AJ*, **151**, 68
- Kopal, Z. 1959, *Close Binary Systems* (New York: Wiley)
- Lomb, N. R. 1976, *Ap&SS*, **39**, 447
- Marigo, P., Girardi, L., Bressan, A., et al. 2017, *ApJ*, **835**, 77
- Mathew, B., & Subramaniam, A. 2011, *BASI*, **39**, 517
- Mennickent, R. E. 2017, *SerAJ*, **194**, 1
- Mennickent, R. E., & Rosales, J. A. 2018, *IBVS*, **63**, 6248
- Mennickent, R. E., & Rosales, J. A. 2019, *IBVS*, **63**, 6268
- Mennickent, R. E., Djurašević, G., Kołaczowski, Z., & Michalska, G. 2012, *MNRAS*, **421**, 862
- Mennickent, R. E., Otero, S., & Kołaczowski, Z. 2016, *MNRAS*, **455**, 1728
- Mennickent, R. E., Pietrzyński, G., Diaz, M., & Gieren, W. 2003, *A&A*, **339**, L47
- Nataf, D. M., Gould, A., Fouqué, P., et al. 2013, *ApJ*, **769**, 88
- Ness, M., & Freeman, K. 2016, *PASA*, **33**, e022
- Pawlak, M., Graczyk, D., Soszyński, I., et al. 2013, *AcAau*, **63**, 323
- Peters, G. J. 1994, in *ASP Conf. Ser.*, **56**, *Interacting Binary Stars*, ed. Allen W. Shafter (San Francisco, CA: ASP), 384
- Poleski, R., Soszyński, I., Udalski, A., et al. 2010, *AcA*, **60**, 179
- Roche, E. A. 1873, *Mem. Acad. Sci. Montpellier*, **8**, 235
- Scargle, J. D. 1982, *ApJ*, **263**, 835
- Schleicher, D. R. G., & Mennickent, R. E. 2017, *A&A*, **602**, A109
- Soszyński, I., Pawlak, M., Pietrukowicz, P., et al. 2016, *AcA*, **117**, 405
- Stellingwerf, R. F. 1978, *ApJ*, **224**, 953
- Udalski, A., Szymański, M. K., & Szymański, G. 2015, *AcA*, **65**, 1
- Zechmeister, M., & Kürster, M. 2009, *A&A*, **496**, 577